

Anomalous enhancement of Néel order in the $S = 1/2$ square lattice Heisenberg model under fictitious magnetic field

Takayuki Yokoyama¹ and Yasuhiro Tada^{1,2,*}

¹*Quantum Matter Program, Graduate School of Advanced Science and Engineering, Hiroshima University, Higashihiroshima, Hiroshima 739-8530, Japan*

²*Institute for Solid State Physics, University of Tokyo, Kashiwa 277-8581, Japan*

Fictitious magnetic fields can be introduced in quantum magnets by the strain engineering and the Aharonov-Casher effect. Here, we study impacts of a uniform fictitious magnetic field and corresponding Landau quantization on the Néel order in the $S = 1/2$ Heisenberg model on the square lattice as a prototypical system of quantum magnets. We first analyze the system by using the spin-wave approximation. It is found that the staggered magnetization is enhanced by the fictitious magnetic field and it shows a simple scaling behavior with respect to the magnetic length, in contrast to a naive expectation based on the Dzyaloshinskii-Moriya interaction. We also perform density matrix renormalization group calculations to fully take quantum effects into account and obtain quantitatively more accurate results. The enhancement is found to be anomalously strong and it shows a non-trivial scaling behavior or a fluctuation induced discontinuity. These results are beyond the well known understanding of correlated systems under magnetic fields called the magnetic catalysis.

I. INTRODUCTION

A magnetic field has significant impacts on physical properties not only through the Zeeman effect but also through the orbital effect. The orbital effect is related to the Landau quantization of a band structure and it has been studied mainly for itinerant electron systems. However, a fictitious magnetic field and corresponding Landau quantization can be introduced in electrically charge-neutral insulators. For example, a fictitious magnetic field can be introduced by strain. The strain-induced fictitious magnetic field was first discussed for graphene, where triaxial strain can effectively lead to a non-uniform magnetic field [1, 2]. Similar mechanisms work also for electrically charge neutral quasi-particles such as emergent Majorana fermions and bosonic magnons in quantum spin systems on the honeycomb lattice, because strain generally leads to modulation of hopping integrals and electromagnetic coupling is not necessary [3–8]. The strain-induced fictitious magnetic fields were generalized to other lattices such as Kagome, α - T_3 , and square lattices [9–12].

The other promising approach for realization of a fictitious magnetic field in a quantum magnet is the Aharonov-Casher effect [13, 14]. In a system with the spin-orbit interaction, an electric field adds to momentum of electrons and thus can behave as an $SU(2)$ gauge field in the spin space, which modifies magnetic interactions and leads to Dzyaloshinskii-Moriya like interactions. Such an effect has been evaluated theoretically [15, 16] and examined experimentally for magnets [17, 18]. The fundamental difference between the strain engineering and the Aharonov-Casher effect is that a spatially uniform fictitious magnetic field can be real-

ized and spin rotation symmetry is reduced in the latter. For a one-dimensional spin chain, the Aharonov-Casher effect with a uniform electric field is simply implemented by the twisted boundary condition and field dependence of the spin current in the Heisenberg model was studied with using the Bethe ansatz [19]. In two dimensions, a uniform electric field generates a constant Aharonov-Casher phase in the magnetic interaction, while an electric field gradient can induce a fictitious magnetic flux which leads to Landau quantization of magnons [20–22]. Theoretically, within the spin-wave approximation neglecting magnon interactions, it was shown that magnons under a fictitious magnetic field can have topologically non-trivial bands and exhibit various Hall effects. It was also proposed that a fictitious magnetic field can give rise to the spin Nernst effect of magnons based on the spin-wave approximation [23]. The basic physics behind these interesting transport phenomena is controlling magnon bands, which is called magnonics [24]. In this context, the fictitious magnetic field induced by the Aharonov-Casher effect can be a useful tool for engineering magnons.

However, despite the extensive studies of quantum spin systems with fictitious magnetic fields, their impacts on magnetic orders have not been well understood. Especially, it is a non-trivial problem whether or not the magnon interactions and quantum fluctuations often ignored within the spin-wave approximation are indeed safely negligible. It was shown that, in the $S = 1/2$ Heisenberg model on the honeycomb lattice under a strain induced non-uniform field, the antiferromagnetic order is weakened even around the center of the system and suppression in the quantum Monte Carlo calculations is much stronger than that in the spin-wave approximation, implying the importance of quantum fluctuations [8]. On the other hand, to our knowledge, magnetism under a uniform fictitious magnetic field has not been theoretically explored and the fate of the magnetism is not known. In contrast to strain-induced fields, a fic-

* ytada@hiroshima-u.ac.jp

titious magnetic field by the Aharonov-Casher effect reduces the spin rotation symmetry and thus a magnetic order could show different behaviors from those under strain. For an electric field which is uniform within a plane, the corresponding fictitious vector potential can be approximated by a Dzyaloshinskii-Moriya interaction and it will suppress the Néel order. In presence of an electric field gradient which gives a fictitious magnetic flux, however, validity of such an approximation is subtle and enhancement of the Néel order might be possible. Furthermore, a change of the magnetic order could be strengthened by magnon interactions.

In this study, we discuss effects of uniform fictitious magnetic fields in the $S = 1/2$ Heisenberg model on the square lattice as a prototypical model of quantum spin systems. We first analyze the model using the spin-wave approximation, and next perform density-matrix-renormalization-group (DMRG) calculations to fully take quantum effects into account and obtain quantitatively more accurate results [25–27]. It is found that the Néel order is enhanced by the fictitious magnetic field in contrast to the above-mentioned naive expectation based on the uniform Dzyaloshinskii-Moriya interaction. Furthermore, the DMRG calculation shows much stronger enhancement of the Néel order, which indicates importance of the quantum fluctuations neglected in the spin-wave approximation. We point out that this enhancement could be regarded as a bosonic variant of the magnetic catalysis which has been extensively studied mainly for Dirac fermion systems [28–37]. However, the anomalous enhancement has not been seen in any fermion systems and is beyond the standard magnetic catalysis. The fictitious magnetic field in quantum magnets could provide an interesting platform for the interplay of Landau quantization and interactions.

II. MODEL AND CALCULATION METHOD

We study the $S = 1/2$ antiferromagnetic Heisenberg model on the square lattice (system size $L_x \times L_y$) under a fictitious magnetic flux ϕ as shown in Fig. 1. The magnetic field is uniform over the entire system, $\sum_{ij \in p} \theta_{ij} = 2\pi\phi$ for every plaquette p . Note that the lattice constant is the length unit in our model and there is no distinction between a magnetic field and a magnetic flux per plaquette. The fictitious magnetic field could be realized by an electric field gradient within the plane through the Aharonov-Casher effect or alternatively by an inhomogeneous Dzyaloshinskii-Moriya interaction [20–24]. The Hamiltonian is

$$\mathcal{H} = \sum_{\langle i,j \rangle} \left[\frac{1}{2} (e^{i\theta_{ij}} S_i^+ S_j^- + e^{-i\theta_{ij}} S_i^- S_j^+) + S_i^z S_j^z \right], \quad (1)$$

where $J > 0$ is an antiferromagnetic interaction and $\langle i, j \rangle$ is a pair of nearest-neighbor sites. The S_j^\pm operators are $S_j^\pm = S_j^x \pm iS_j^y$. The present magnetic field is a fictitious

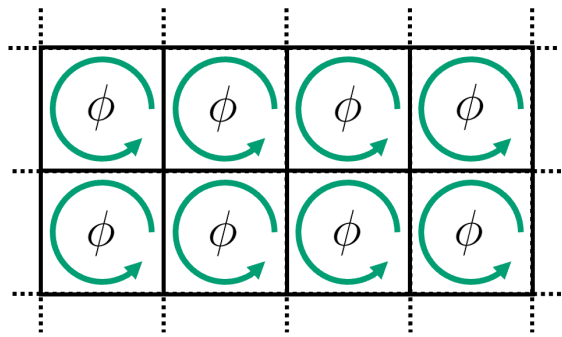


FIG. 1. A schematic picture of the square lattice under the fictitious magnetic flux ϕ per plaquette.

field and the Hamiltonian does not contain a Zeeman term. We introduce the fictitious vector potential θ_{ij} in the Landau gauge as

$$\theta_{ij} = 2\pi\phi \frac{x_i + x_j}{2} (y_i - y_j), \quad (2)$$

where the site position is denoted by $\mathbf{r}_j = (x_j, y_j)$ with $x_j = 0, 1, \dots, L_x - 1$ and $y_j = 0, 1, \dots, L_y - 1$. The Heisenberg model with the vector potential has the $U(1)$ global spin rotation symmetry along the spin z -axis, and the spin π -rotation symmetry along the x -axis combined with the complex conjugation, $z \rightarrow z^*$, $S_j^+ \rightarrow S_j^-$, $S_j^- \rightarrow -S_j^+$, where z is a complex constant. Note that, in the standard notation of the spin operators with the Pauli matrices, the y -component transforms as $S_j^y \rightarrow -S_j^y$ under the complex conjugation. Thus the $SU(2)$ spin rotation symmetry at $\phi = 0$ is reduced to $U(1) \times \mathbb{Z}_2$ symmetry in presence of $\phi \neq 0$ (the \mathbb{Z}_2 symmetry is anti-unitary). The combined π -rotation symmetry is spontaneously broken in the z -axis Néel ordered state. In this study, we use two system geometries, namely a torus and a cylinder, where there are no boundary effects in the former while the latter is convenient for discussions on small fluxes. We impose the periodic boundary condition for both x, y -directions in the torus geometry, for which the flux is quantized as $\phi = p/L_x$ with $p \in \mathbb{Z}$. On the other hand, the cylinder geometry has the open (periodic) boundary condition for the $x(y)$ -direction. The flux is quantized as $\phi = p/\{(L_x - 1)L_y\}$ for which the (projective) mirror symmetry $x \rightarrow L_x - x$ is kept in the cylinder.

In this study, we first apply the spin-wave approximation which is a standard method to describe low-energy properties of quantum magnets. The Hamiltonian is approximated within quadratic terms in the boson operators and interactions between the magnons are neglected (see Appendix A). In the spin-wave approximation, both of the torus and the cylinder geometries are used depending on physical quantities considered and ranges of the fictitious magnetic flux. Next, we perform the DMRG calculation in the cylinder geometry to obtain more accurate results. The quantum fluctuations arising from the magnon interaction neglected in the spin-wave ap-

proximation are taken into account in the DMRG calculation. The aspect ratio is chosen as $(L_x, L_y) = (2L, L)$ with the system size $L = 6, 8, 10$. The bond dimension is $\chi = 800 \sim 3200$ and the truncation error is $\epsilon < 10^{-5}$. [25–27].

III. CALCULATION RESULTS

In this section, we show the calculation results of the spin-wave approximation and the DMRG at zero temperature. They give qualitatively consistent results, but there is significant quantitative difference. To have an insight into the results of DMRG calculation, we give a brief discussion based on the magnetic catalysis.

A. Spin-wave approximation

In the spin-wave approximation, we suppose that the classical ground state at $\phi = 0$ is the Néel ordered state in the spin z -axis. The staggered magnetic moment m_s will increase if the \mathbb{Z}_2 symmetry breaking state becomes more stable, while m_s would decrease if the $U(1)$ symmetry breaking takes place. In the latter case, the z -axis Néel ansatz is inappropriate and the spin-wave approximation based on this ansatz state would not work. More precisely, the energy spectrum of magnons will have imaginary components when the spin-wave approximation becomes invalid. A failure of the spin-wave approximation implies instability of the Néel ordered ansatz and a different order may be realized in the ground state.

We first calculate energy spectrum of the magnons and investigate how the magnon excitations depend on the fictitious magnetic flux ϕ . Figure 2 shows the energy spectrum calculated by the spin-wave approximation for various magnetic fluxes $0 \leq \phi \leq 1$. The magnon spectrum shows a Hofstadter butterfly as in a

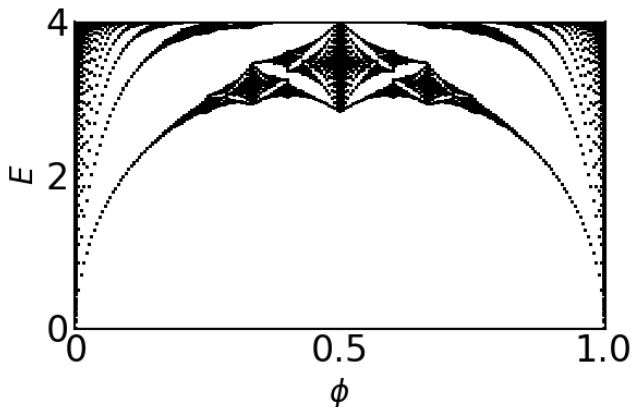


FIG. 2. Magnon energy spectrum under the fictitious magnetic flux ϕ within the spin-wave approximation. The system size is $L_x = L_y = 200$ in the torus geometry.

free fermion system, as demonstrated in the previous studies [22, 23, 38]. Note that the calculated magnon energy is always real (non-imaginary) for all ϕ , which implies that the z -axis Néel ground state is stable under the fictitious magnetic field. If the z -axis Néel state were unstable under some fluxes, the magnon energy would take complex values. One can see that the magnon excitation acquires an energy gap under the magnetic field $\phi \neq 0$. The magnon excitation gap ΔE (the smallest magnon excitation energy) behaves as $\Delta E \propto \sqrt{\phi}$ for small magnetic fluxes $0 < \phi \lesssim 0.01$ as shown in Figs. 3(a) and (b), which is consistent with the long wavelength behavior described by the Klein-Gordon equation [23]. The $\Delta E \propto \sqrt{\phi}$ dependence can be understood by a simple dimensional analysis of the linear spectra in the momentum space $\Delta E \propto k$ at $\phi = 0$. Indeed, $\Delta E \propto k \propto 1/L$ for the system size L and one can just replace L with the magnetic length $l_B = 1/\sqrt{\phi}$ to obtain $\Delta E \propto 1/l_B = \sqrt{\phi}$. Note that the long-wavelength limit of the magnon spectrum is effectively described by the Klein-Gordon equation and there is no zero mode ($\Delta E = 0$) in sharp contrast to Dirac fermions at charge neutrality. The non-zero magnon gap implies that any excitations from the ground state are gapped since the magnons are elementary excitations in the Heisenberg model. The correlation length will be given by $\xi \sim v/\Delta E \propto l_B$ where v is the speed of the magnon excitation, and the system is governed by this length scale.

Next, we calculate the Néel order parameter m_s given by

$$m_s = \frac{1}{N} \sum_j \langle S_j^z \rangle (-1)^j, \quad (3)$$

where we use the cylinder geometry since it allows small fluxes. N is the number of sites in the summation and it is restricted to the $N = L \times L$ sites in the middle of the system for the cylinder geometry with $(L_x, L_y) = (2L, L)$ to suppress contributions from the open boundary. Note that the spin-wave approximation works quite well for the Heisenberg model at $\phi = 0$ and it gives $m_s \simeq 0.303$ in the thermodynamic limit which is very close to $m_s \simeq 0.306 \sim 0.309$ obtained by the extensive numerical calculations [39–45]. Figure 4(a) shows the Néel order parameter m_s under the fictitious magnetic flux ϕ . We find that the Néel order parameter is enhanced from the zero flux value $m_s(0) \simeq 0.303$ and it reaches $m_s \sim 0.41$ at large fluxes. Once the enhanced m_s has been obtained, it can be naturally understood from the gapped magnon spectrum in analogy to an Ising-like system at $\phi = 0$ where magnons are gapped and correspondingly m_s is large. Since zero-point motion of the magnons leads to the suppression of m_s from the classical value $m_{\max} = 0.5$ within the spin-wave approximation, a magnon gap would generally imply increase of m_s . At the same time, however, the enhanced Néel order may be non-trivial, once one notices that the Hamiltonian (1) partly includes a non-uniform Dzyaloshinskii-Moriya interaction in the spin xy -plane when $e^{i\theta_{ij}}$ is simply Taylor

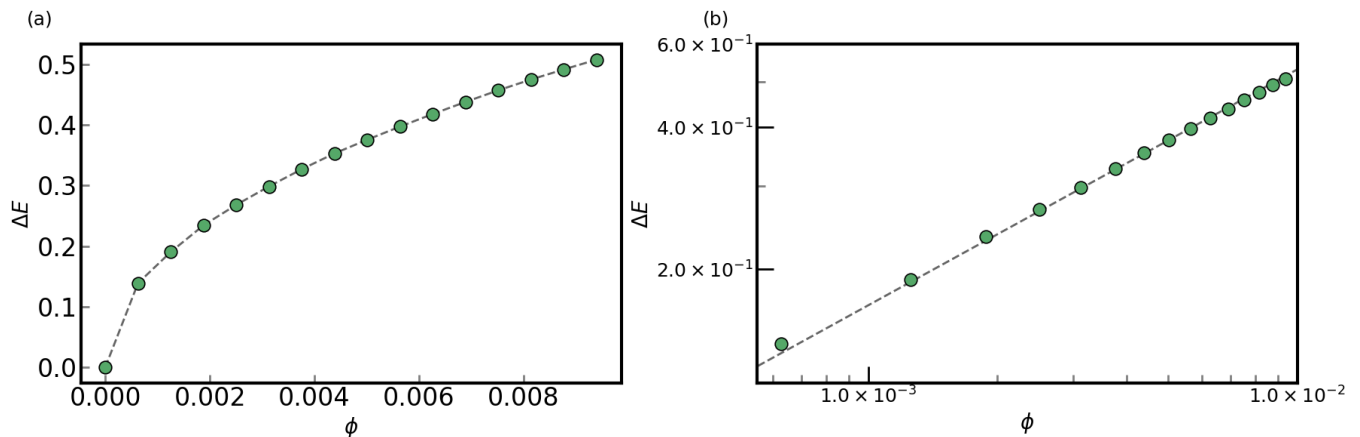


FIG. 3. Magnon energy gap for small values of the fictitious magnetic field (a) in the linear scale and (b) in the logarithmic scale. The system size is $L_x = L_y = 100$ sites with the cylinder geometry. The dashed curve in (b) is $\Delta E \sim \sqrt{\phi}$. Small deviation from the exact $\Delta E \sim \sqrt{\phi}$ behavior is considered to be a finite size effect.

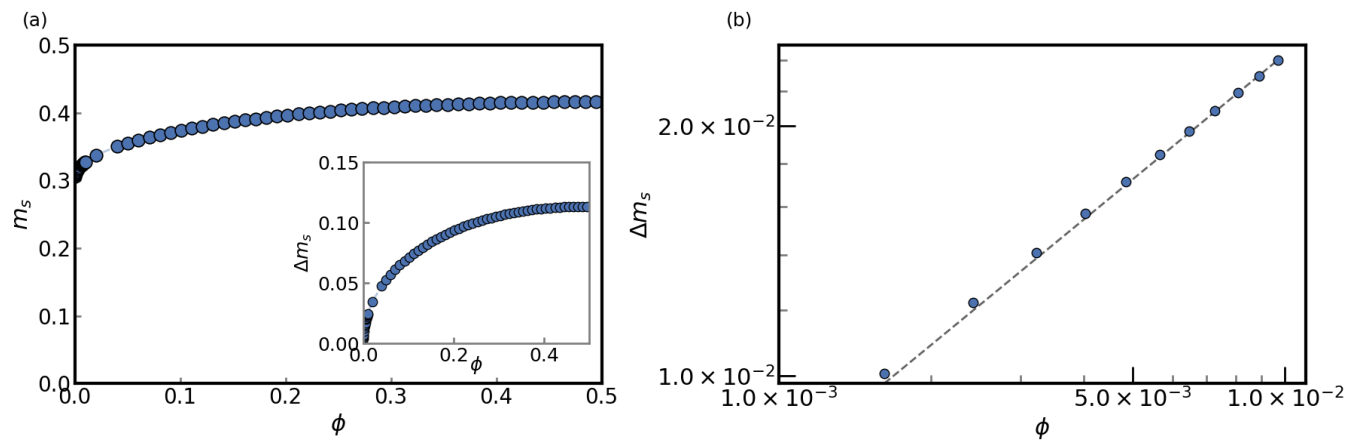


FIG. 4. (a) Néel order parameter m_s calculated by the spin-wave approximation in the cylinder geometry for the system size $L_x = 100, L_y = 50$. The inset is the difference Δm_s for small fluxes $0 \leq \phi \lesssim 0.01$. (b) Logarithmic scale plot of Δm_s . The dashed line represents $\Delta m_s \propto \sqrt{\phi}$.

expanded up to the lowest order in ϕ . A uniform xy -Dzyaloshinskii-Moriya interaction is known to destabilize the z -axis Néel order, and one might naively expect that the non-uniform Dzyaloshinskii-Moriya interaction has a similar influence. The enhancement of the Néel order in our calculation suggests that it is important to fully take the Landau quantization into account beyond the naive Taylor expansion.

Interestingly, the staggered moment exhibits a scaling behavior. To see this, we define an excess Néel magnetization measured from m_s at $\phi = 0$,

$$\Delta m_s(\phi) = m_s(\phi) - m_s(0), \quad (4)$$

where $m_s(0) = 0.303$. As shown in Fig. 4(b), the difference Δm_s behaves as $\Delta m_s \propto \sqrt{\phi} = l_B^{-1}$ for small magnetic fluxes. Generally, a physical quantity could be expanded in integer powers of l_B^{-1} (with possible logarithmic corrections) within the spin-wave approximation

which is a free bosons description, since the l_B is the cut off scale for the gapped magnons as mentioned above. The $\Delta m_s \propto l_B^{-1}$ dependence is the leading order behavior with respect to l_B . In this sense, Δm_s can be regarded as a correction to $m_s(0)$ due to the finite magnetic length l_B just like the conventional finite size effect for a system with a linear size L [46]. In Appendix B, we extend our discussion to the XXZ model with Ising anisotropy and demonstrate that the system is indeed governed by the magnetic length l_B based on a finite-size scaling analysis. Note that ΔE and Δm_s slightly deviate from the exact power-law with the exponent $1/2$ in the very small region of $0 \leq \phi \lesssim 0.01$. Two possible reasons for this deviation can be considered. The first one is that the magnetic length l_B may exceed the system size L , potentially leading to non-critical behaviors in the weak magnetic field region. The second is a technical issue regarding instability in the spin-wave calculation due to

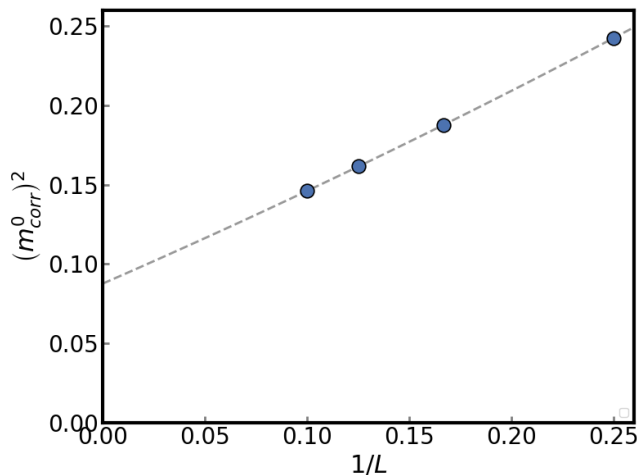


FIG. 5. $(m_{\text{corr}}^0)^2$ plotted versus $1/L$ for $L = 4, 6, 8, 10$. The dashed curve is a polynomial fitting, $m = m_0 + m_1/L + m_2/L^2 + m_3/L^3$, which gives $(m_0)^2 = 0.087(1)$ and $(m_0) = 0.295(3)$.

specific modes which are connected to the gapless modes at $\phi = 0$. The deviation is not physically meaningful, because these problems can be avoided in the thermodynamic limit.

From the spin-wave calculation of the z -axis Néel order, one can see that the fictitious magnetic field effectively enhances the Ising interaction $J S_i^z S_j^z$. One can compare the results above for the Heisenberg model at $\phi \neq 0$ with the previous results for the XXZ model at $\phi = 0$, since these two models have the same symmetry $U(1) \times \mathbb{Z}_2$. The XY interaction is denoted by J_{xy} and the Ising interaction by $J_z \geq J_{xy}$. In the XXZ model at $\phi = 0$, the spin-wave approximation gives $\Delta E(J_z) \propto \sqrt{J_z - J_{xy}}$ and $\Delta m_s(J_z) \propto \sqrt{J_z - J_{xy}}$ in the leading order [47, 48]. The $\sqrt{J_z - J_{xy}}$ dependence in these quantities has been confirmed by various methods [44, 45], and one would naively expect that the $\sqrt{\phi}$ dependence in the Heisenberg model at $\phi \neq 0$ holds beyond the spin-wave approximation as well. However, magnon interactions are neglected in the spin-wave approximation and validity of this approximation may be non-trivial in the present system. To resolve this problem, we will discuss the DMRG calculations in the next section.

B. DMRG calculation

In the DMRG calculation, we focus on the correlation function for the z -axis Néel order,

$$(m_{\text{corr}}^z)^2 = \frac{1}{N^2} \sum_{j,k} \langle S_j^z S_k^z \rangle e^{i\mathbf{q} \cdot (\mathbf{r}_j - \mathbf{r}_k)}, \quad (5)$$

where $\mathbf{r}_j = (x_j, y_j)$ and $\mathbf{q} = (\pi, \pi)$. The summation is restricted to the $N = L \times L$ sites in the middle

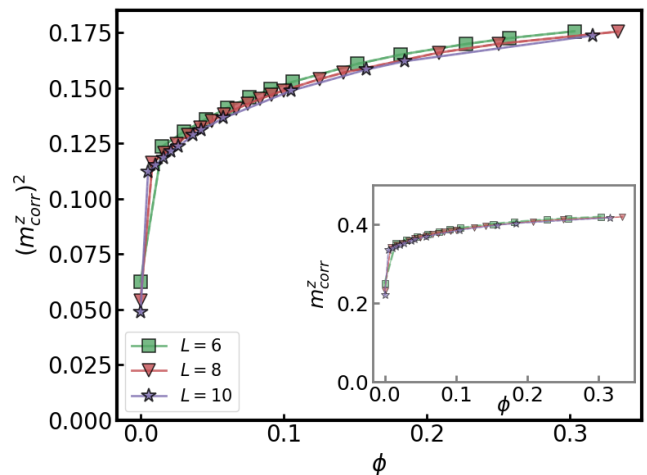


FIG. 6. Néel correlation function $(m_{\text{corr}}^z)^2$ as a function of ϕ for various system sizes $(L_x, L_y) = (2L, L)$ calculated by DMRG. The yellow square is for $L = 6$, and the green triangle is for $L = 8$, and the orange cross is for $L = 10$.

of the $(L_x, L_y) = (2L, L)$ cylinder system to suppress contributions from the open boundaries. We first evaluate $(m_{\text{corr}}^z)^2$ in absence of the magnetic field. The system is $SU(2)$ symmetric at $\phi = 0$ and thus the Néel correlations are isotropic, $(m_{\text{corr}}^x)^2 = (m_{\text{corr}}^y)^2 = (m_{\text{corr}}^z)^2 \equiv (m_{\text{corr}}^0)^2/3$, where $(m_{\text{corr}}^{x,y})^2$ are defined similarly to Eq. (5). We show $(m_{\text{corr}}^z)^2$ at $\phi = 0$ in Fig. 5 for system sizes $L = 4, 6, 8, 10$. The polynomial fitting of the results for the finite size systems gives $m_{\text{corr}}^0 = 0.295(3)$ in the thermodynamic limit $L \rightarrow \infty$. The obtained m_{corr}^0 is slightly smaller than the previous results $m_{\text{corr}}^0 = 0.306 \sim 0.308$ evaluated by several numerical methods [39–45], because the system sizes used in our extrapolation are limited to $L = 4 \sim 10$. Nevertheless, the deviation is at most few percents and we have confirmed that it has only negligible influence in the following discussions for $\phi \neq 0$ (see Appendix C). We find that the calculated ground state at $\phi \neq 0$ is essentially a uniform state with the long range Néel order similarly to the results within the spin-wave approximation in the previous section, although there are some deviations around the open boundaries. The ground state belongs to the $S_{\text{tot}}^z = \sum_i S_i^z = 0$ sector.

Figure 6 shows the calculated $(m_{\text{corr}}^z)^2$ as a function of the fictitious magnetic flux ϕ . Similarly to the results by the spin-wave approximation in the previous section, the Néel magnetization is enhanced by the flux. Besides, the system size dependence becomes smaller as ϕ increases, which is qualitatively consistent with the finite correlation length $\sim l_B$ of the gapped magnons in the spin-wave approximation since finite size effects are generally suppressed in a gapped system. However, the two results obtained by the spin-wave approximation and the DMRG are significantly different in a quantitative manner. Namely, the enhancement of the Néel magnetization

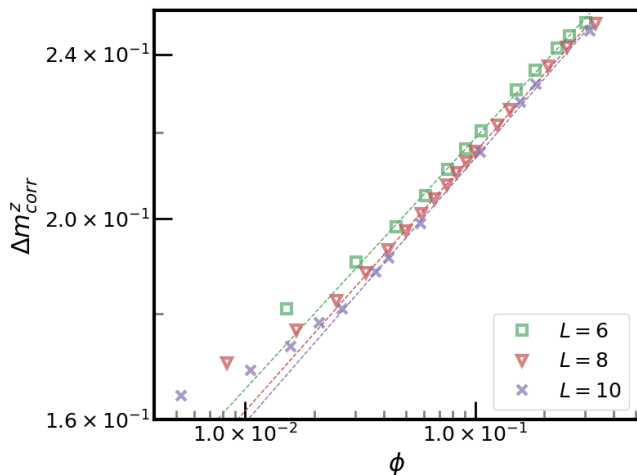


FIG. 7. Scaling plot of $\Delta m_{\text{corr}}^z(\phi)$ with $L = 6, 8, 10$. The power law fitting is represented by the dashed lines.

around $\phi = 0$ in the DMRG calculation is much stronger than that in the spin-wave approximation. This behavior could be described by a power-law function with a small exponent or by a discontinuous function.

To understand detailed behaviors under the assumption that $m_{\text{corr}}^z(\phi)$ is continuous at $\phi = 0$, we introduce the difference

$$\Delta m_{\text{corr}}^z(\phi) = m_{\text{corr}}^z(\phi) - m_{\text{corr}}^z(0), \quad (6)$$

where $m_{\text{corr}}^z(0) = m_{\text{corr}}^0(0)/\sqrt{3} \equiv 0.295/\sqrt{3}$. Note that $\Delta m_{\text{corr}}^z(0) = 0$ in the thermodynamic limit by definition, (See also Appendix C.) We show a logarithmic scale plot of the difference Δm_{corr}^z in Fig. 7. It has only small L -dependence for relatively large magnetic fields as already mentioned. In this field region, Δm_{corr}^z exhibits a scaling behavior,

$$\Delta m_{\text{corr}}^z = C \cdot \phi^n, \quad (7)$$

where the prefactor C only weakly depends on the system size L . This scaling behavior holds above a crossover scale ϕ_L for each system size, and it is roughly estimated to be $\phi_6 \simeq 0.05, \phi_8 \simeq 0.04, \phi_{10} \simeq 0.03$. We obtain the exponent n and the prefactor C for each system size L , and they are extrapolated for $L \rightarrow \infty$ (Fig. 8). These results are summarized in Table I. Numerically, the crossover scale ϕ_L decreases as the system size increases, $\phi_6 > \phi_8 > \phi_{10}$. Although we naively expect that $\phi_L \rightarrow 0$ as $L \rightarrow \infty$, it could converge to some non-zero value ϕ_∞ and a different scaling exponent might be obtained for $\phi < \phi_\infty$. In any case, the obtained exponent $n \simeq 0.136$ for $L = 6, 8, 10$ gives an upper bound since the slope in Fig. 7 for $\phi < \phi_0$ is smaller than that for $\phi > \phi_0$. Therefore, we conclude that the fictitious magnetic field leads to the anomalously strong enhancement of the Néel order with the scaling behavior $\Delta m_{\text{corr}}^z \propto \phi^n$ with $n \lesssim 0.136$. Note that the above discussion is based

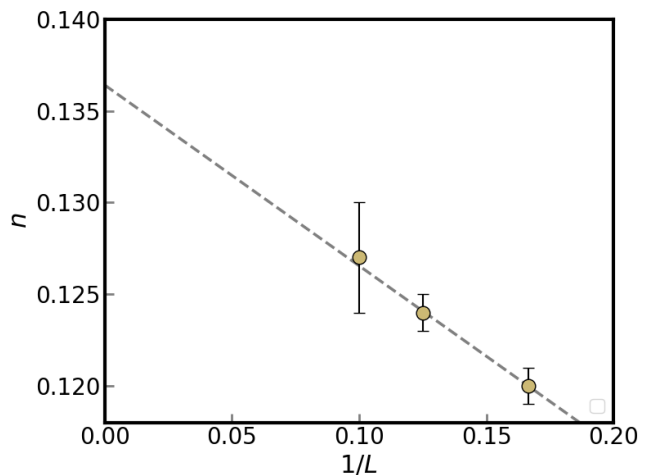


FIG. 8. The exponent n plotted versus $1/L$ with $L = 6, 8, 10$. The dashed line represents the linear fitting with weighted least squares, which gives $n \simeq 0.136$ in the thermodynamic limit.

system size L	exponent n	prefactor C
$L = 6$	0.120(1)	0.288(1)
$L = 8$	0.124(1)	0.286(1)
$L = 10$	0.127(3)	0.286(2)
$L \rightarrow \infty$	0.136(0)	~ 0.286

TABLE I. Results of the power-law fitting Eq. (7). The exponent n in the thermodynamic limit is estimated with weighted least squares. The prefactor C is estimated to be nearly 0.286 in the thermodynamic limit, as the finite size effect is negligible within the present numerical accuracy.

on the assumption that the enhancement of $m_{\text{corr}}^z(\phi)$ is continuous and can be described by a power-law function. If $m_{\text{corr}}^z(\phi)$ is discontinuous at $\phi = 0$, the enhancement is even stronger than any power-law behavior. Since the Néel order is continuous within the spin-wave approximation as demonstrated in the previous section, a possible discontinuity will be understood as a fluctuation-induced discontinuity. In any case, our DMRG calculation suggests importance of the magnon interactions neglected in the spin-wave approximation. This may be somewhat counter-intuitive, because magnon interactions are usually negligible at low temperatures where there are few thermally excited magnons. Indeed, the significant difference between the spin-wave results and the DMRG results is highly non-trivial even when compared with the magnetic catalysis in any known systems, as discussed in the next section.

C. Discussion based on magnetic catalysis

Here, we give a brief alternative discussion for the anomalous enhancement of the Néel order in the Heisen-

berg model under the fictitious magnetic fields. We will argue that it is beyond the well known magnetic catalysis for correlated systems under magnetic fields [28–37]. Our discussion is based on the hard-core bosons which are equivalent to $S = 1/2$ spins via the relations $c_j = S_j^-$ and $n_j = c_j^\dagger c_j = S_j^z + 1/2$, where c_j is the boson annihilation operator. The Heisenberg model at $S_{\text{tot}}^z = 0$ can be rewritten as the extended Hubbard model of hard-core bosons at half-filling,

$$\mathcal{H}_B = t \sum_{\langle i,j \rangle} \left(e^{i\theta_{ij}} c_i^\dagger c_j + e^{-i\theta_{ij}} c_j^\dagger c_i \right) + V \sum_{\langle i,j \rangle} \left(n_i - \frac{1}{2} \right) \left(n_j - \frac{1}{2} \right) \quad (8)$$

with $2t = V = J$. The hard-core condition ($n_j = 0, 1$) can be regarded as the strong coupling limit of the on-site Hubbard interaction $U n_j (n_j - 1)$. The boson model has the particle number $U(1)$ symmetry and the anti-unitary particle-hole symmetry $z \rightarrow z^*, c_j \rightarrow c_j^\dagger, n_j \rightarrow 1 - n_j$ corresponding to the $U(1) \times \mathbb{Z}_2$ spin rotation symmetry of the Heisenberg model. The particle-hole symmetry is spontaneously broken in the charge-density wave state as in the z -axis Néel state of the Heisenberg model.

For the hard-core boson model, the fictitious magnetic field is nothing but a standard magnetic field for charged bosons or may be regarded as an artificial field in cold atoms [49–51]. The magnetic field leads to the Landau quantization of single-particle energies and the band structure becomes flat, which means that the hopping integral t is effectively reduced. Consequently the interaction $V n_i n_j$ can be enhanced compared to the kinetic energy. To be more precise, the particles are localized within a length scale $\sim l_B$, and the system size effectively becomes $\sim l_B \times l_B$ in two dimensions, where the correlation effects are amplified due to the spatial confinement. Such a mechanism for enhanced correlation effects by magnetic fields is called magnetic catalysis and it has been extensively studied mainly for fermion systems [28–37]. The magnetic catalysis has been examined also for bosons at finite temperature [52, 53]. In this picture, it is natural to have an enhanced charge density wave order of the hard-core bosons for the Hamiltonian (8). However, there is a striking difference between the magnetic catalysis for the present system and the known systems in a quantitative manner.

One can compare the DMRG results of the Heisenberg model which is located at a bicritical fixed point of the renormalization group [54] with the known magnetic catalysis for interacting fermion systems at critical fixed points. In the $(2+1)$ -dimensional Dirac fermions, the magnetic catalysis of an order parameter Δm at the semimetal-insulator transition point behaves as $\Delta m \propto l_B^{-\beta/\nu} = \phi^{\beta/2\nu}$ [37], and it is described by the exactly same scaling form $\Delta m(L) \propto L^{-\beta/\nu}$ for a finite size system with the linear size L at $\phi = 0$ [55–59]. The exponents β and ν are defined as $\Delta m \sim g^\beta$ and $\xi \sim g^{-\nu}$ with g

and ξ the reduced interaction and the correlation length, respectively, when there are no other finite size effects. They are $\beta = \nu = 1$ in the mean field approximation, and the order parameter behaves as $\Delta m \sim l_B^{-1} = \sqrt{\phi}$. According to the extensive numerical studies, the critical exponents are $(\beta, \nu) \simeq (0.53, 0.80) \sim (0.63, 0.78)$ for a \mathbb{Z}_2 symmetry breaking order parameter [58, 59], and correspondingly, $\Delta m \sim l_B^{-0.81 \sim -0.66} = \phi^{0.33 \sim 0.40}$ [37]. This means that the quantum fluctuations neglected in the mean field approximations play important roles in the magnetic catalysis especially at a quantum critical point, and they lead to strong enhancement of the order parameter by the magnetic field.

We naively expect that the magnetic length l_B is a scaling variable in the present hard-core bosons as well, if the order parameter is continuous at $\phi = 0$. (More precisely, we consider the singular part of the ground state energy measured from that at $g = l_B^{-1} = 0$, $\Delta \varepsilon(h, g, l_B^{-1}) = \varepsilon(h, g, l_B^{-1}) - \varepsilon(h, 0, 0)$, where h is an external field conjugate to the Néel magnetization and $g = (V - V_c)/V_c$.) Indeed, in the spin-wave approximation, the Néel order parameter behaves as $\Delta m_s^z \sim l_B^{-\beta/\nu} = 1/l_B$ similarly to the well known finite size correction $\Delta m_s^z \sim 1/L$ [44–46] (see also Appendix B). This is fully consistent with the physical picture of the critical magnetic catalysis for the hard-core bosons with $\beta = \nu = 1/2$. However, the critical behavior of the magnetic catalysis in the DMRG calculation is much stronger, $\Delta m_{\text{corr}}^z \sim \phi^{0.136} = l_B^{-0.272}$, if it is continuous at $\phi = 0$. Obviously, the simple correspondence between l_B and L does not hold, and the scaling dimension of ϕ in $\Delta \varepsilon(h, g, \phi)$ is $\lambda_\phi \neq -1/2$. This implies that the anomalous enhancement of Δm_{corr}^z cannot be understood based on the standard magnetic catalysis. This may be related to the fact that the fictitious magnetic field leads not only to the Landau quantization but also to the symmetry reduction from $SU(2)$ to $U(1) \times \mathbb{Z}_2$, which is distinct from the electromagnetic field. The Bosonic nature of the constituent particles would also be important for the anomalous scaling.

Another possibility is that Δm_{corr}^z has the fluctuation induced discontinuity at $\phi = 0$, as already mentioned. In any case, the anomalous enhancement of the Néel order (or the charge density wave order in terms of the bosons) is beyond the known magnetic catalysis. It is an interesting future problem to fully clarify the origin and mechanism of the anomalous behavior of $\Delta m_{\text{corr}}^z(\phi)$.

IV. SUMMARY

We have studied impacts of the fictitious magnetic flux ϕ in the $S = 1/2$ Heisenberg model on the square lattice. Within the spin-wave approximation neglecting the magnon interaction, we found that the magnon excitation gap is $\Delta E \sim \sqrt{\phi}$ in agreement with the field theory description in the previous study. As a result, the Néel antiferromagnetic order is enhanced by the application of a fictitious magnetic flux and it shows a scal-

ing behavior $\Delta m_s \sim \sqrt{\phi}$. This is reasonable because of the magnon gap, but in contrast to a naive expectation based on the Dzyaloshinskii-Moriya interaction appearing in the lowest-order expansion of the Aharonov-Casher phase. We also performed the DMRG calculations to fully take the magnon interactions and quantum fluctuations into account. Interestingly, we identified a much stronger enhancement of the Néel order with the scaling behavior $\Delta m_{\text{corr}}^z \sim \phi^{0.136}$ or possibly a fluctuation-induced discontinuous enhancement. The anomalous enhancement compared with the spin-wave approximation clearly suggests importance of the quantum fluctuations of the Heisenberg model which is critical. An alternative picture for the anomalous enhancement was discussed based on the magnetic catalysis for critical systems by rewriting the Heisenberg model as an interacting hard-core boson model. The magnetic catalysis in the present system is stronger than that in any fermion systems and is beyond the standard magnetic catalysis. The quantum spin systems are an interesting platform for the interplay of the Landau quantization and interactions.

ACKNOWLEDGMENTS

The DMRG calculations are performed with the use of ITensor.jl [27]. We thank Shunsuke C. Furuya and Takahiro Misawa for fruitful discussions. This study is supported by JSPS KAKENHI Grant No.22K03513.

Appendix A: Details of the spin-wave approximation

In the spin-wave approximation, we use the Holstein-Primakoff transformation [60]. The annihilation (creation) operators of the hard-core bosons $a_i^{(\dagger)}, b_i^{(\dagger)}$ are introduced for the sublattices A and B. In a spin- S system, the spin operators are written as

$$S_i^+ = \sqrt{2S - a_i^\dagger a_i} \cdot a_i, \quad S_i^z = S - a_i^\dagger a_i \quad (\text{A1})$$

on the A sublattice and

$$S_i^+ = b_i^\dagger \sqrt{2S - b_i^\dagger b_i}, \quad S_i^z = -S + b_i^\dagger b_i \quad (\text{A2})$$

on the B sublattice. Then the Hamiltonian is approximated up to quadratic terms as

$$\mathcal{H}_{\text{sw}} = JS \sum_{\langle i,j \rangle} \left(a_i^\dagger a_i + b_i^\dagger b_i + e^{i\theta_{ij}} a_i^\dagger b_j^\dagger + e^{-i\theta_{ij}} a_i b_j \right), \quad (\text{A3})$$

where we have neglected interactions between the bosons. The Hamiltonian in the real space basis can be straightforwardly diagonalized. Since the spin-wave Hamiltonian has the magnetic translation symmetry on a torus, physical quantities are also translationally symmetric. It turns out that translational symmetry is kept in the bulk even

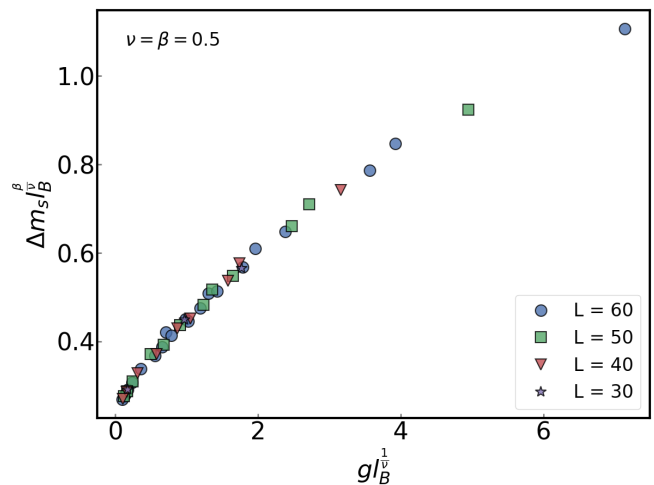


FIG. 9. Scaling plot of $\Delta m_s(g, l_B)$ for $g = (J_z - J_{xy})/J_{xy}$ and $l_B = 1/\sqrt{\phi}$. The parameters are $0 \leq \phi \lesssim 0.01$ and $0 \leq g \lesssim 0.01$. The critical exponents are fixed as $\beta = \nu = 1/2$.

for cylinder geometry. Based on this observation, we perform the Fourier transformation in the y -direction in the cylinder geometry. The Hamiltonian is written as

$$\mathcal{H}_{\text{sw}} = \sum_{k_y} M_{k_y}^\dagger H_{k_y} M_{k_y}, \quad (\text{A4})$$

$$M_{k_y} = [a_{x_1, k_y}^\dagger, a_{x_2, k_y}^\dagger, \dots, b_{x_1, k_y}, b_{x_2, k_y}]^T. \quad (\text{A5})$$

The matrix H_{k_y} can be diagonalized by a Bogoliubov transformation, and physical quantities can be calculated based on the eigenvectors of H_{k_y} [61, 62].

Appendix B: Finite-size scaling within spin-wave approximation

To establish that the magnetic length is the dominant cut off scale in the Heisenberg model under the fictitious magnetic field within the spin-wave approximation, we extend our discussion to the XXZ model and perform a finite-size analysis. We consider the XXZ model under a fictitious magnetic field,

$$\mathcal{H} = \sum_{\langle i,j \rangle} \left[\frac{J_{xy}}{2} (e^{i\theta_{ij}} S_i^+ S_j^- + e^{-i\theta_{ij}} S_i^- S_j^+) + J_z S_i^z S_j^z \right], \quad (\text{B1})$$

where $J_z/J_{xy} \geq 1$. The Heisenberg point $J_z = J_{xy}$ is SU(2) symmetric and is located at a bicritical point [54], whereas the ground state is Néel ordered along the z -axis under the condition $J_z > J_{xy}$. Near the critical point $J_z = J_{xy}$, we suppose that the deference Δm_s is described by a scaling function f ,

$$\Delta m_s(g, l_B) = l_B^{-\beta/\nu} f(g l_B^{1/\nu}) \quad (\text{B2})$$

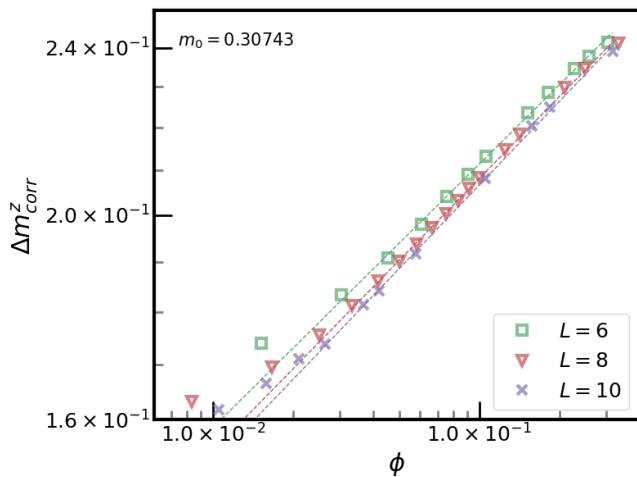


FIG. 10. Scaling plot of $\Delta m_{\text{corr}}^z(\phi)$. The zero field value is $m_{\text{corr}}^0 = 0.30743$ obtained in the previous quantum Monte Carlo study [41]. The dashed lines are power law fitting.

where $g = (J_z - J_{xy})/J_{xy}$ and β, ν are the critical exponents at $\phi = 0$ for the divergence $\Delta m_s(g, l_B \rightarrow \infty) \sim g^\beta$ and the correlation length $\xi(g, l_B \rightarrow \infty) = g^{-\nu}$. Note that we use l_B instead of L for the finite-size scaling analysis, since l_B is considered to be the dominant length scale rather than the system size L when $l_B < L$. In the previous works at $\phi = 0$, the spin-wave approximation gives the enhancement of the Néel order $\Delta m_s(J_z) \propto \sqrt{J_z - J_{xy}}$ and energy gap $\Delta E \propto \sqrt{J_z - J_{xy}}$ in the leading order [47, 48]. The same critical behaviors have been obtained also by the extensive numerical calculations [44, 45]. These studies give the critical exponents $\beta = 0.5$ and also $\nu = 0.5$ under the assumption that the dynamical critical exponent is $z = 1$ since the correlation length ξ scales as $\xi^z \sim \frac{1}{\Delta E}$. Figure 9 shows the finite- l_B scaling with the fixed critical exponents $\beta = \nu = 1/2$. We

see that the numerical data successfully collapse onto a single curve, and the finite- l_B scaling indeed holds. Thus the two length scales l_B and L are interchangeable within the spin-wave approximation, which may be reasonable. However, this equivalence is broken in the DMRG results where the full quantum fluctuations are taken into account as discussed in the main text.

Appendix C: Robustness of power-law fitting for m_{corr}^0

In the main text, the zero field value of the Néel magnetization $m_{\text{corr}}^0 = 0.2985$ is used for the discussions of Δm_{corr}^z . To check robustness of our discussion, we perform the same power-law fitting using a different zero-field value, $m_{\text{corr}}^0 = 0.30743$ obtained in the previous quantum Monte Carlo study [41]. Figure 10 shows the logarithmic scale plot of Δm_{corr}^z versus ϕ using $m_{\text{corr}}^0 = 0.30743$, similar to Fig. 7 in the main text. The power-law behavior can be seen for $\phi > \phi_0$, where the crossover scale is $\phi_0 = 0.05$. The calculation results are summarized in Table II. The exponent n and the prefactor C are extrapolated to $n \simeq 0.141$, $C \simeq 0.275$, and they are close to those obtained in the main text. These results indicate that the slight deviation of the background m_{corr}^0 is negligible in the power-law fitting.

System size L	exponent n	prefactor C
$L = 6$	0.124(2)	0.281(1)
$L = 8$	0.128(1)	0.280(1)
$L = 10$	0.131(3)	0.279(2)
$L \rightarrow \infty$	0.141(1)	0.275(3)

TABLE II. Results of power-law fitting Eq. (7) with $m_{\text{corr}}^0 = 0.30743$. The values of n and C in the thermodynamic limit are evaluated by linear-fitting with weighted least squares.

-
- [1] F. Guinea, M. Katsnelson, and A. Geim, Energy gaps and a zero-field quantum hall effect in graphene by strain engineering, *Nat. Phys.* **6**, 30 (2010).
- [2] N. Levy, S. A. Burke, K. L. Meaker, M. Panlasigui, A. Zettl, F. Guinea, A. H. C. Neto, and M. F. Crommie, Strain-induced pseudo-magnetic fields greater than 300 tesla in graphene nanobubbles, *Science* **329**, 544 (2010).
- [3] S. Rachel, L. Fritz, and M. Vojta, Landau levels of majorana fermions in a spin liquid, *Phys. Rev. Lett.* **116**, 167201 (2016).
- [4] M. M. Nayga, S. Rachel, and M. Vojta, Magnon Landau levels and emergent supersymmetry in strained antiferromagnets, *Phys. Rev. Lett.* **123**, 207204 (2019).
- [5] T. Liu and Z. Shi, Magnon quantum anomalies in Weyl ferromagnets, *Phys. Rev. B* **99**, 214413 (2019).
- [6] M. N. Chernodub and M. A. H. Vozmediano, Chiral sound waves in strained Weyl semimetals, *Phys. Rev. Res.* **1**, 032040 (2019).
- [7] J. Sun, H. Guo, and S. Feng, Magnon Landau levels in the strained antiferromagnetic honeycomb nanoribbons, *Phys. Rev. Res.* **3**, 043223 (2021).
- [8] J. Sun, N. Ma, T. Ying, H. Guo, and S. Feng, Quantum Monte Carlo study of honeycomb antiferromagnets under a triaxial strain, *Phys. Rev. B* **104**, 125117 (2021).
- [9] T. Liu, Strain-induced pseudomagnetic field and quantum oscillations in kagome crystals, *Phys. Rev. B* **102**, 045151 (2020).
- [10] J. Sun, T. Liu, Y. Du, and H. Guo, Strain-induced pseudo magnetic field in the $\alpha - T_3$ lattice, *Phys. Rev. B* **106**, 155417 (2022).
- [11] A. Filusch and H. Fehske, Tunable valley filtering in dynamically strained $\alpha - \square_3$ lattices, *Phys. Rev. B* **106**, 245106 (2022).

- [12] J. Sun, X. Zhu, T. Liu, S. Feng, and H. Guo, Pseudomagnetic fields in square lattices, *Phys. Rev. B* **108**, 205149 (2023).
- [13] Y. Aharonov and A. Casher, Topological quantum effects for neutral particles, *Phys. Rev. Lett.* **53**, 319 (1984).
- [14] Y. Avishai and Y. B. Band, Aharonov–bohm and aharonov–casher effects in meso-scopic physics: A brief review (2023), [arXiv:2302.06300 \[cond-mat.mes-hall\]](https://arxiv.org/abs/2302.06300).
- [15] T. Liu and G. Vignale, Electric control of spin currents and spin-wave logic, *Phys. Rev. Lett.* **106**, 247203 (2011).
- [16] A. Marmodoro, S. Mankovsky, H. Ebert, J. Minár, and O. c. v. Šipr, Electric field control of magnons in magnetic thin films: Ab initio predictions for two-dimensional metallic heterostructures, *Phys. Rev. B* **105**, 174411 (2022).
- [17] X. Zhang, T. Liu, M. E. Flatté, and H. X. Tang, Electric-field coupling to spin waves in a centrosymmetric ferrite, *Phys. Rev. Lett.* **113**, 037202 (2014).
- [18] R. O. Serha, V. I. Vasyuchka, A. A. Serga, and B. Hillebrands, Towards an experimental proof of the magnonic aharonov-casher effect, *Phys. Rev. B* **108**, L220404 (2023).
- [19] A. A. Zvyagin and P. Schlottmann, Aharonov-casher effect in the heisenberg spin chain with many impurities, *Phys. Rev. B* **52**, 6569 (1995).
- [20] K. Nakata, J. Klinovaja, and D. Loss, Magnonic quantum hall effect and wiedemann-franz law, *Phys. Rev. B* **95**, 125429 (2017).
- [21] K. Nakata, S. K. Kim, J. Klinovaja, and D. Loss, Magnonic topological insulators in antiferromagnets, *Phys. Rev. B* **96**, 224414 (2017).
- [22] S. Owerre, Magnonic floquet hofstadter butterfly, *Annals of Physics* **399**, 93 (2018).
- [23] B. Li and A. A. Kovalev, Magnon landau levels and spin responses in antiferromagnets, *Phys. Rev. Lett.* **125**, 257201 (2020).
- [24] P. A. McClarty, Topological magnons: A review, *Annals of Physics* **13**, 171 (2022).
- [25] S. R. White, Density matrix formulation for quantum renormalization groups, *Phys. Rev. Lett.* **69**, 2863 (1992).
- [26] E. Stoudenmire and S. R. White, Studying two-dimensional systems with the density matrix renormalization group, *Annual Review of Condensed Matter Physics* **3**, 111 (2012).
- [27] M. Fishman, S. R. White, and E. M. Stoudenmire, The ITensor Software Library for Tensor Network Calculations, *SciPost Phys. Codebases*, 4 (2022).
- [28] V. A. Miransky and I. A. Shovkovy, Quantum field theory in a magnetic field: From quantum chromodynamics to graphene and dirac semimetals, *Physics Reports* **576**, 1 (2015).
- [29] V. P. Gusynin, V. A. Miransky, and I. A. Shovkovy, Catalysis of dynamical flavor symmetry breaking by a magnetic field in $2 + 1$ dimensions, *Phys. Rev. Lett.* **73**, 3499 (1994).
- [30] V. P. Gusynin, V. A. Miransky, and I. A. Shovkovy, Dynamical flavor symmetry breaking by a magnetic field in $2+1$ dimensions, *Phys. Rev. D* **52**, 4718 (1995).
- [31] I. V. Krive and S. A. Naftulin, Dynamical symmetry breaking and phase transitions in a three-dimensional gross-neveu model in a strong magnetic field, *Phys. Rev. D* **46**, 2737 (1992).
- [32] D. D. Scherer and H. Gies, Renormalization group study of magnetic catalysis in the $3d$ gross-neveu model, *Phys. Rev. B* **85**, 195417 (2012).
- [33] J. J. Lenz, M. Mandl, and A. Wipf, Magnetic catalysis in the $(2 + 1)$ -dimensional gross-neveu model, *Phys. Rev. D* **107**, 094505 (2023).
- [34] V. Gusynin, V. Miransky, and I. Shovkovy, Theory of the magnetic catalysis of chiral symmetry breaking in qed, *Nuclear Physics B* **563**, 361 (1999).
- [35] E. V. Gorbar, V. P. Gusynin, V. A. Miransky, and I. A. Shovkovy, Magnetic field driven metal-insulator phase transition in planar systems, *Phys. Rev. B* **66**, 045108 (2002).
- [36] F. Semenoff, Gordon W. Zhou, Magnetic catalysis and quantum hall ferromagnetism in weakly coupled graphene, *Journal of High Energy Physics* **2011**, 10.1007/JHEP07(2011)037 (2011).
- [37] Y. Tada, Quantum criticality of magnetic catalysis in two-dimensional correlated dirac fermions, *Phys. Rev. Res.* **2**, 033363 (2020).
- [38] D. R. Hofstadter, Energy levels and wave functions of bloch electrons in rational and irrational magnetic fields, *Phys. Rev. B* **14**, 2239 (1976).
- [39] A. W. Sandvik and C. J. Hamer, Ground-state parameters, finite-size scaling, and low-temperature properties of the two-dimensional $s = \frac{1}{2}$ XY model, *Phys. Rev. B* **60**, 6588 (1999).
- [40] S. R. White and A. L. Chernyshev, Néel order in square and triangular lattice heisenberg models, *Phys. Rev. Lett.* **99**, 127004 (2007).
- [41] A. W. Sandvik and H. G. Evertz, Loop updates for variational and projector quantum monte carlo simulations in the valence-bond basis, *Phys. Rev. B* **82**, 024407 (2010).
- [42] R. Bishop, P. Li, R. Zinke, R. Darradi, J. Richter, D. Farnell, and J. Schulenburg, The spin-half xxz antiferromagnet on the square lattice revisited: A high-order coupled cluster treatment, *Journal of Magnetism and Magnetic Materials* **428**, 178 (2017).
- [43] M. Kadosawa, M. Nakamura, Y. Ohta, and S. Nishimoto, Study of staggered magnetization in the spin- s square-lattice heisenberg model using spiral boundary conditions, *Journal of the Physical Society of Japan* **92**, 023701 (2023), <https://doi.org/10.7566/JPSJ.92.023701>.
- [44] M. R. Walther, D.-B. Hering, G. S. Uhrig, and K. P. Schmidt, Continuous similarity transformation for critical phenomena: Easy-axis antiferromagnetic xxz model, *Phys. Rev. Res.* **5**, 013132 (2023).
- [45] N. Caci, D.-B. Hering, M. R. Walther, K. P. Schmidt, S. Wessel, and G. S. Uhrig, Quantitative description of long-range order in the spin- $\frac{1}{2}$ xxz antiferromagnet on the square lattice, *Phys. Rev. B* **110**, 054411 (2024).
- [46] H. Neuberger and T. Ziman, Finite-size effects in heisenberg antiferromagnets, *Phys. Rev. B* **39**, 2608 (1989).
- [47] Z. Weihong, J. Oitmaa, and C. J. Hamer, Second-order spin-wave results for the quantum xxz and xy models with anisotropy, *Phys. Rev. B* **44**, 11869 (1991).
- [48] C. J. Hamer, Z. Weihong, and P. Arndt, Third-order spin-wave theory for the heisenberg antiferromagnet, *Phys. Rev. B* **46**, 6276 (1992).
- [49] M. Aidelsburger, M. Atala, M. Lohse, J. T. Barreiro, B. Paredes, and I. Bloch, Realization of the hofstadter hamiltonian with ultracold atoms in optical lattices, *Phys. Rev. Lett.* **111**, 185301 (2013).
- [50] H. Miyake, G. A. Siviloglou, C. J. Kennedy, W. C. Burton, and W. Ketterle, Realizing the harper hamiltonian with laser-assisted tunneling in optical lattices, *Phys.*

- Rev. Lett.* **111**, 185302 (2013).
- [51] F. A. An, E. J. Meier, and B. Gadway, Direct observation of chiral currents and magnetic reflection in atomic flux lattices, *Science Advances* **3**, e1602685 (2017), <https://www.science.org/doi/pdf/10.1126/sciadv.1602685>.
- [52] H. Rojas, Bose-einstein condensation may occur in a constant magnetic field, *Physics Letters B* **379**, 148 (1996).
- [53] A. Ayala, M. Loewe, J. C. Rojas, and C. Villavicencio, Magnetic catalysis of a charged bose-einstein condensate, *Phys. Rev. D* **86**, 076006 (2012).
- [54] D. R. Nelson and R. A. Pelcovits, Momentum-shell recursion relations, anisotropic spins, and liquid crystals in $2 + \epsilon$ dimensions, *Phys. Rev. B* **16**, 2191 (1977).
- [55] S. Sorella and E. Tosatti, Semi-metal-insulator transition of the hubbard model in the honeycomb lattice, *Europhysics Letters* **19**, 699 (1992).
- [56] F. F. Assaad and I. F. Herbut, Pinning the order: The nature of quantum criticality in the hubbard model on honeycomb lattice, *Phys. Rev. X* **3**, 031010 (2013).
- [57] Y. Otsuka, S. Yunoki, and S. Sorella, Universal quantum criticality in the metal-insulator transition of two-dimensional interacting dirac electrons, *Phys. Rev. X* **6**, 011029 (2016).
- [58] L. Wang, P. Corboz, and M. Troyer, Fermionic quantum critical point of spinless fermions on a honeycomb lattice, *New Journal of Physics* **16**, 103008 (2014).
- [59] Z.-X. Li, Y.-F. Jiang, and H. Yao, Fermion-sign-free majorana-quantum-monte-carlo studies of quantum critical phenomena of dirac fermions in two dimensions, *New Journal of Physics* **17**, 085003 (2015).
- [60] T. Holstein and H. Primakoff, Field dependence of the intrinsic domain magnetization of a ferromagnet, *Phys. Rev.* **58**, 1098 (1940).
- [61] J. Colpa, Diagonalization of the quadratic boson hamiltonian, *Physica A: Statistical Mechanics and its Applications* **93**, 327 (1978).
- [62] M. wen Xiao, *Theory of transformation for the diagonalization of quadratic hamiltonians* (2009), arXiv:0908.0787 [math-ph].